Current Biology, Vol. 14, 953–964, June 8, 2004, ©2004 Elsevier Ltd. All rights reserved. DOI 10.1016/j.cub.2004.05.053

Spindle Checkpoint Protein Dynamics at Kinetochores in Living Cells

Bonnie J. Howell, Ben Moree, Emily M. Farrar, Scott Stewart, Guowei Fang, and E.D. Salmon*
Department of Biology, CB#3280
607 Fordham Hall
University of North Carolina
Chapel Hill, North Carolina 27599

Summary

Background: To test current models for how unattached and untense kinetochores prevent Cdc20 activation of the anaphase-promoting complex/cyclosome (APC/C) throughout the spindle and the cytoplasm, we used GFP fusions and live-cell imaging to quantify the abundance and dynamics of spindle checkpoint proteins Mad1, Mad2, Bub1, BubR1, Mps1, and Cdc20 at kinetochores during mitosis in living PtK_2 cells.
Results: Unattached kinetochores in prometaphase bound on average only a small fraction (estimated at 500–5000 molecules) of the total cellular pool of each spindle checkpoint protein. Measurements of fluorescence recovery after photobleaching (FRAP) showed that GFP-Cdc20 and GFP-BubR1 exhibit biphasic exponential kinetics at unattached kinetochores, with ~50% displaying very fast kinetics ($t_{1/2}$ of ~1–3 s) and ~50% displaying slower kinetics similar to the single exponential kinetics of GFP-Mad2 and GFP-Bub3 ($t_{1/2}$ of 21–23 s). The slower phase of GFP-Cdc20 likely represents complex formation with Mad2 since it was tension insensitive and, unlike the fast phase, it was absent at metaphase kinetochores that lack Mad2 but retain Cdc20 and was absent at unattached prometaphase kinetochores for the Cdc20 derivative GFP-$Cdc20_{\Delta 1-167}$, which lacks the major Mad2 binding domain but retains kinetochore localization. GFP-Mps1 exhibited single exponential kinetics at unattached kinetochores with a $t_{1/2}$ of ~10 s, whereas most GFP-Mad1 and GFP-Bub1 were much more stable components.
Conclusions: Our data support catalytic models of checkpoint activation where Mad1 and Bub1 are mainly resident, Mad2 free of Mad1, BubR1 and Bub3 free of Bub1, Cdc20, and Mps1 dynamically exchange as part of the diffuse wait-anaphase signal; and Mad2 interacts with Cdc20 at unattached kinetochores.

Introduction

The spindle checkpoint is an intracellular signaling pathway that delays anaphase until all chromosomes become aligned at the spindle equator in metaphase. In mammalian tissue cells, the checkpoint is essential for preventing chromosome missegregation and aneuploidy, an outcome leading to cancer or birth defects [1]. Key components of the spindle checkpoint include Mad1, Mad2, Bub1, BubR1 (Mad3 in budding yeast), Bub3, and Mps1, and all these proteins localize to unattached kinetochores during early mitosis, become reduced upon microtubule attachment and tension [2, 3], and are required for mitotic arrest in the presence of spindle poisons in both yeast and vertebrates [4].

Early studies have shown kinetochores lacking a full complement of kinetochore microtubules or tension are checkpoint active, and a single unattached kinetochore can prevent anaphase onset [5]. Checkpoint-active kinetochores inhibit anaphase by blocking Cdc20 activation of the anaphase-promoting complex/cyclosome (APC/C), a ubiquitin ligase that polyubinquinates proteins and targets them for proteolysis by the 26S proteosome. In checkpoint-active cytoplasm, Mad2 and BubR1 have key roles in preventing APC/C^{Cdc20} activity. Both Mad2 and BubR1 bind directly to Cdc20 in vitro and either independently or cooperatively inhibit polyubiquination of APC/C^{Cdc20} substrates [6–10]. In yeast, *Xenopus*, and mammalian tissue cells, checkpoint activation induces various Cdc20-containing complexes including Cdc20-Mad2, Cdc20-BubR1-Bub3, and Cdc20-Mad2-BubR1-Bub3, also known as the mitotic checkpoint complex (MCC) [11–13]. In mammalian tissue cells, more than half of the MCC or its subcomplexes appear bound to the APC/C [14, 15]. In anaphase cells or extracts, MCC or its subcomplexes disappear, and a complex of Cdc20 and APC/C is predominant (reviewed by [4, 16]).

Two current models exist for how unattached kinetochores produce a diffuse signal that prevents activation of APC^{Cdc20} in the cytoplasm. The "catalytic model" proposes that Cdc20 becomes inactivated in the cytoplasm by transient association of Cdc20 or its inhibitors with unattached kinetochores [14, 15, 17, 18]. In support of this model, we previously showed kinetochore bound Mad2 exchanges with cytoplasmic pools with a half-life of ~24 s [18]. Kallio et al. also reported rapid exchange of Cdc20 at kinetochores with a half-life of ~6s [15]. It is not known, however, if other spindle checkpoint proteins (particularly the MCC components BubR1 and Bub3) also exchange rapidly at checkpoint-active kinetochores. If the MCC or its subcomplexes are generated or exchange at kinetochores, then the dynamics of their individual components should share common kinetic features. In contrast, neither Mad1, Bub1, nor Mps1 are part of the MCC or its subcomplexes, and these proteins may not exchange rapidly and may serve as resident binding sites at kinetochores [3, 4].

A second model (the "APC/C sensitization model") proposes checkpoint-active kinetochores sensitize the APC/C to inhibition by cytoplasmic MCC, perhaps by phosphorylation [11]. This could be achieved by APC/C rapidly exchanging with kinetochores since there is some, but conflicting, evidence for APC/C localization to kinetochores [19–22]. Mps1 also binds the APC/C, and thus it might be the diffusible signal from an unattached kinetochore that sensitizes APC/C to inhibition

*Correspondence: tsalmon@email.unc.edu

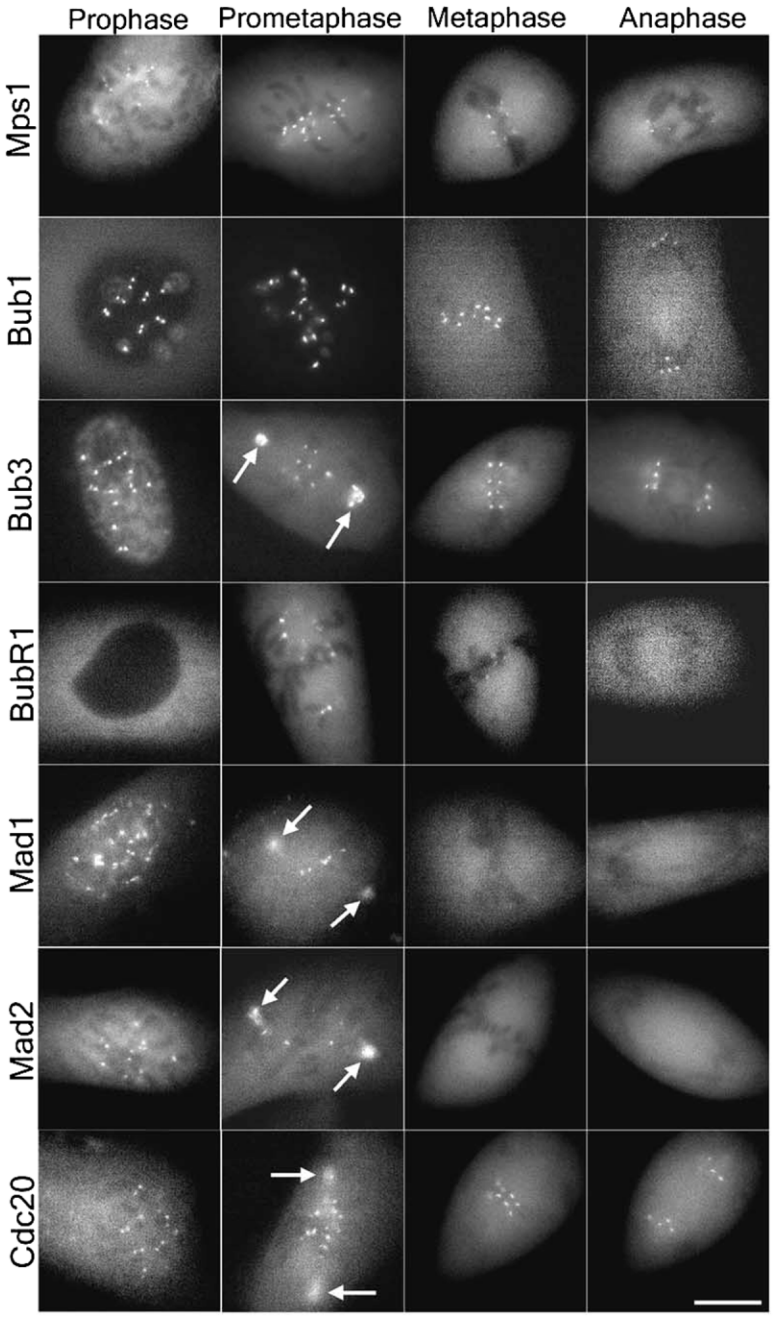

Figure 1. Localization of GFP Fusions of Spindle Checkpoint Components in Mitotic PtK_2 Cells

Mps1, Bub1, Bub3, Mad1, Mad2, and Cdc20 localize to unattached kinetochores in prophase, whereas BubR1 localizes to kinetochores after nuclear envelope breakdown. Bub1, Bub3, Cdc20, and to a lesser extent, Mps1, remain detectable at kinetochores throughout anaphase whereas Mad1, Mad2, and BubR1 deplete during metaphase. Bub3, Mad1, Mad2, and Cdc20 show prominent spindle pole localization (arrows) during prometaphase, but not in metaphase. Scale bar, 10 μm.

by MCC [23]. If so, then Mps1 should exchange rapidly between kinetochores and the cytoplasm. Mps1 is also known to be required for Mad1/Mad2 localization to kinetochores [23, 24]. Thus, if Mps1 provides the sole binding site for Mad1 at kinetochores, it should be equal or more stable than Mad1.

To test between the above possibilities and to provide better mechanistic understanding of the spindle checkpoint, we used GFP chimeras, live-cell imaging, and FRAP [18, 25] to follow the dynamics of spindle checkpoint proteins and Cdc20 at kinetochores in living PtK_2 cells.

Results

Live-Cell Analysis of Spindle Checkpoint Proteins and Cdc20 in PtK_2 Cells

We created GFP fusions, transiently transfected them into PtK_2 cells, and performed assays 2–3 days after transfection. Figure 1 and Movies 1–5 are representative images. Only cells expressing GFP chimeras barely detectable by the dark-adapted eye in the microscope were recorded in the assays used in this paper. Although not studied in detail (with few exceptions), cells expressing GFP-fusion proteins at the barely detectable level

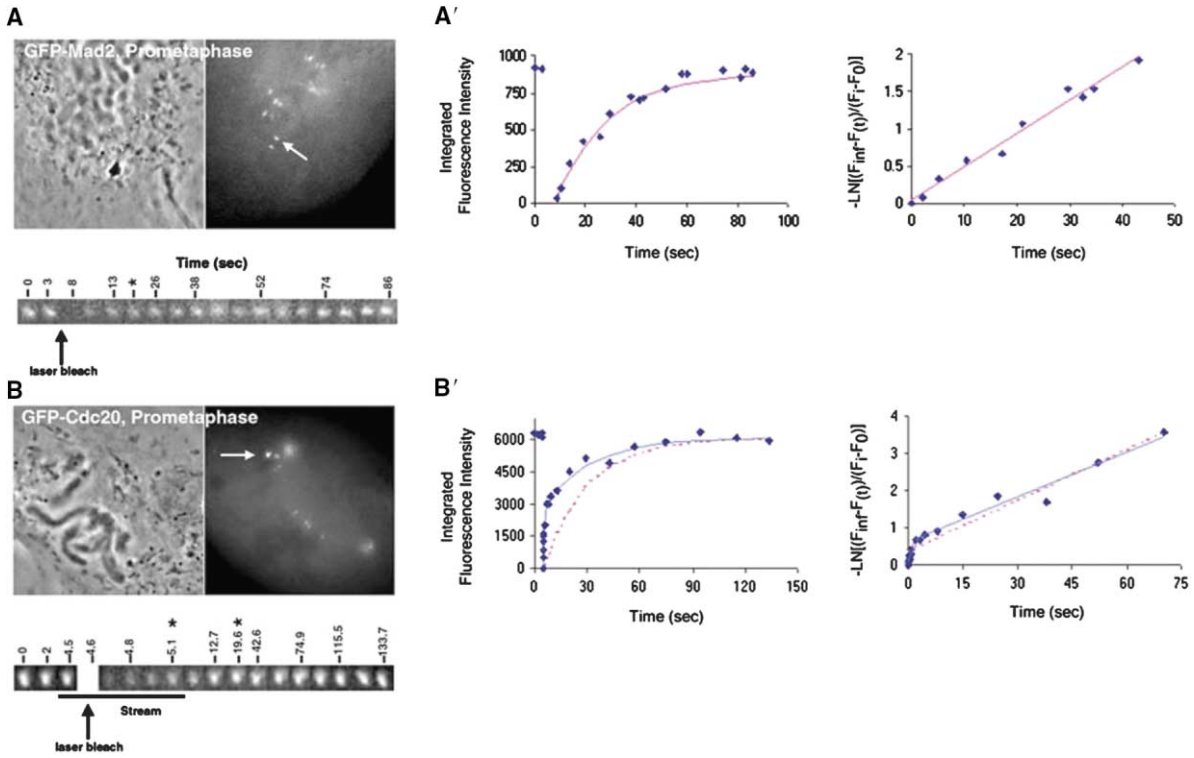

Figure 2. FRAP Analysis of GFP-Mad2 and GFP-Cdc20 at Unattached Kinetochores in PtK_2 Cells

Representative phase and fluorescent images from GFP-Mad2 (A) and GFP-Cdc20 (B) prometaphase PtK_2 cells showing the targeted kinetochore. Montaged images of kinetochore fluorescence before and after photobleaching are shown. (A′ and B′) Plots of integrated kinetochore fluorescence intensity and the natural log plot against time are shown. Mad2 (A′) fit a single exponential (pink line) whereas Cdc20 (B′) displayed biphasic kinetics and best fit the sum of two exponentials (blue line). See Experimental Procedures for FRAP analysis.

exhibited no obvious abnormalities in chromosome movements and mitotic progression (see Experimental Procedures and Movies). Based on measurements for GFP-Mad2 and GFP-Mad1, cells with barely detectable fluorescence had GFP-Mad2 at about 1.5 times the endogenous level while GFP-Mad1 was about 4-fold the endogenous level. The difference likely is related to the 3-fold higher endogenous concentration of Mad2 compared to Mad1 and likely represents the range of overexpression of GFP-fusion proteins in the cells chosen for analysis in our experiments (Figures S1 and S2 and Supplemental Discussion). Consistent with previous immunofluorescence studies in mammalian tissue culture cells [2, 14, 23, 24, 26–29], these low-level GFP fusions to Bub1, Bub3, Mad1, Mad2, Mps1, and Cdc20 concentrated at unattached kinetochores during late prophase, whereas BubR1 appeared at kinetochores around the time of nuclear envelope breakdown (Figure 1). All were reduced by 4-fold or more at kinetochores by late metaphase except for Cdc20, which diminished 1.7-fold by early metaphase and persisted at this level into anaphase (see below). We found Mad1 and Bub3 concentrated at spindle poles in prometaphase cells, like noted previously for Mad2 [17, 18, 31] and Cdc20 [15], but Bub1 and BubR1 showed little, if any, pole localization (Figure 1). Interestingly, Bub3 and Cdc20 spindle pole localization diminished during metaphase despite persistence of these components on metaphase kinetochores. Mps1 showed weak pole localization consistent with other studies [23, 28, 31]. Our limits of detection and dynamic range for fluorescence quantification was about 1/20 the intensity of unattached prometaphase kinetochores above background cytoplasmic fluorescence (Figure S3).

Mad2, BubR1, Bub3, Mps1, and Cdc20 Rapidly Cycle through Unattached Kinetochores

To identify which spindle checkpoint components are dynamically exchanging at checkpoint-active kinetochores, we performed FRAP analysis of kinetochore protein dynamics by using a brief 25 ms laser pulse to photobleach the GFP molecules of proteins bound to unattached kinetochores. In our previous Mad2 studies, we showed that photobleaching bound fluorophore did not disrupt normal binding to the kinetochore and that cells progressed normally through mitosis [18]. A sample photobleaching experiment can be seen in Figure 2A. Fluorescence recovered as subunits with bleached GFP dissociated and subunits with unbleached GFP from the cytoplasmic pool associated at the same steady-state rate (see [25] for theory). Our CCD camera was able to record images during and following photobleaching at 100–200 ms intervals so we could record rapid rates of fluorescence recovery. Because the size of the focused beam was small (0.8 μm diameter Gaussian beam profile at half-maximal intensity), bleached cytoplasmic GFP

Table 1. FRAP Analysis of Checkpoint Components at Unattached and Attached Kinetochores in Living PtK_2 Cells

		Early Prometaphase (Unattached, Unaligned KTs)			Metaphase (Attached, Aligned KTs)		
		$t_{1/2}$[a] (s)	Percentage R[a]	n	$t_{1/2}$[a] (s)	Percentage R[a]	n
GFPMps1		13 ± 3	92 ± 14	11	5 ± 2	98 ± 13	10
GFPBub1		57 ± 24	65 ± 18	9	25 ± 16	56 ± 20	13
GFPBub3		21 ± 4	95 ± 13	10	7 ± 3	85 ± 14	9
GFPBubR1	Fast phase	3 ± 3	46 ± 10	8	1 ± 1	65 ± 38	6
	Slow phase	21 ± 9	54 ± 10	8	10 ± 3	42 ± 38	4
GFPMad1		16 ± 7	29 ± 15	7	NA	NA	NA
GFPMad2		19 ± 7	91 ± 17	13	NA	NA	NA
GFPCdc20	Fast phase	1 ± 1	53 ± 17	10	2 ± 2	95 ± 12	8
	Slow phase	23 ± 10	47 ± 17	10			
$GFPCdc20_{\Delta 1-167}$		2 ± 1	93 ± 11	12	2 ± 1	91 ± 10	12
GFPCdc20 (10μM taxol)		ND	ND		2 ± 1	88 ± 12	8

[a] The exponetial kinetics of FRAP were analyzed by calculating the normalized unrecovered fluorescence at each time point, $(F_{inf} - F(t))/(F_{inf} - F_0)$, where F_{inf} is the average maximal fluorescence recovery, and F_0 is the fluorescence immediately after photobleaching.
The normalized data was fit to either $\exp(-kt)$ from the slope of the ln plot of the normalized data Microsoft Excel or fit to a double exponential $R_f\exp(-k_f t) + R_s\exp(-k_s t)$ by using the Regression Wizard function in SigmaPlot, where f and s are the fast and slow components. Abbreviations: n, number of cells; NA, not applicable; and ND, not determined.

subunits within the targeted region are completely replaced by unbleached GFP subunits by diffusional movement within a 200 ms recording interval ([18]; Figure S4). For Mad2, fluorescence recovery at the bleached kinetochore was fit by single exponential kinetics (one amplitude constant and one rate constant, Figure 2A′). The steady-state dissociation constant, k_d, was determined from the slope of the natural log plot in Figure 2A′. The half-life of fluorescence recovery equals ln(2)/k_d and the average value for Mad2 at unattached kinetochores was $t_{1/2}$ ~19s (Table 1). Average fluorescence recovery occurred for ~91% of bleached GFP-Mad2 fluorescence (the exponential amplitude constant), similar to that measured previously for PtK_1 cells [18].

GFP-Cdc20 dynamics at unattached kinetochores in PtK_2 cells were rapid (Figure 2B) as predicted from the recent Kallio et al. [15] study in LLCPK cells. However, our higher temporal and spatial resolution revealed that GFP-Cdc20 fluorescence recovery exhibited biphasic kinetics that were poorly fit by a single exponential and fit much better using the sum of two exponentials (each with different amplitude and rate constants (Figure 2B′). On average, 53% of fluorescence recovery occurred with a $t_{1/2}$ of ~1 s, while 47% occurred with a $t_{1/2}$ of ~23 s, a half-life similar to the turnover of Mad2 ($p < 0.01$; Table 1). Similar biphasic kinetics and average kinetic parameters were found for unattached kinetochores in prophase and nocodazole-treated cells (data not shown).

Next, we compared the turnover rates of two other MCC components, Bub3 and BubR1, to the exchange rates of Mad2 and Cdc20 at unattached kinetochores (Figure 3, Table 1; Figure S5). We were interested in testing whether these components also dynamically cycle through kinetochores, like Mad2 and Cdc20, and if so, whether they displayed monophasic or biphasic recoveries. We found Bub3 displayed monophasic recovery with a turnover similar to Mad2 at unattached kinetochores ($t_{1/2}$ of ~21 s with ~95% recovery, $p < 0.01$; Figure 3; Table 1; Figure S5). BubR1, like Cdc20, also displayed biphasic recovery (Figure 3; Table 1; Figure S5). The slow component of BubR1 ($t_{1/2}$ of ~21 s and 54% recovery) exchanged at a rate similar to Mad2, Bub3, and to the slow component of Cdc20 ($p < 0.01$; Figure 3; Table 1; Figure S5). The fast component for BubR1 displayed a half-life of ~3s with 46% recovery. Similar biphasic rates were seen for BubR1 in prophase and nocodazole-treated cells (data not shown).

To test if Mps1 might contribute to a diffusible signal between the kinetochore and APC/C in the cytoplasm as proposed by Liu et al. [23], we examined the dynamics of GFP-Mps1 at kinetochores. GFP-Mps1 displayed monophasic recovery with a $t_{1/2}$ of ~13 s and ~92% recovery (Figure 3; Table 1; Figure S5). The 13 s half-life was statistically different ($p < 0.01$) than the longer half-lives of the slow phases of Cdc20 and BubR1 and to those of Mad2 and Bub3.

Mad1 and Bub1 Exhibit Stability at Unattached Kinetochores

In contrast to the other spindle-checkpoint components, we found GFP-Mad1 and GFP-Bub1 were much more stable at unattached prometaphase kinetochores either because of slower turnover rates and/or decreased fluorescence recovery percentages. For example, about 70% of the GFP-Mad1 population did not exchange with the cytoplasmic pool over a 10–15 min period (Figure 3; Table 1; Figure S5). The other 30% had a half-life similar to Mad2 at unattached kinetochores ($t_{1/2}$ of ~16 s, $p < 0.01$; Table 1). GFP-Bub1 also displayed relatively slow dynamics at unattached kinetochores ($t_{1/2}$ of ~57 s and 65% fluorescence recovery; Figure 3; Table 1; Figure S5). Thus, Mad1 and Bub1 are much more stable components of unattached kinetochores compared to the MCC components Mad2, Bub3, BubR1, and Cdc20.

Protein Dynamics Increase for Proteins that Persist at Metaphase Kinetochores

Some checkpoint components (e.g., Bub3, Bub1, and Mps1) and Cdc20 persisted at sufficient levels at metaphase kinetochores for FRAP analysis (Figure 1; Table 2). We found all proteins tested exhibited increased turn-

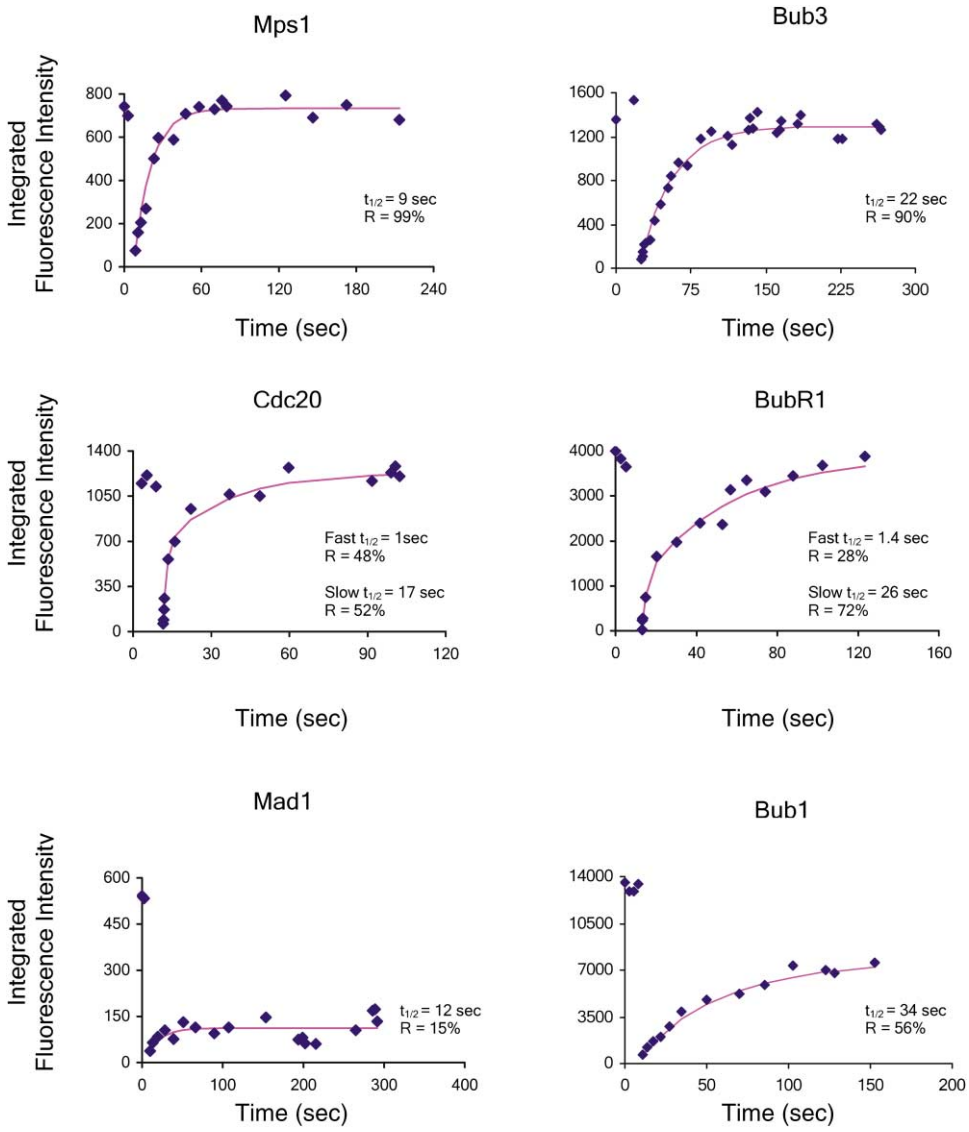

Figure 3. FRAP Analysis of GFP Fusions to Mps1, Bub3, BubR1, Cdc20, Mad1, and Bub1 at Unattached Kinetochores in Mitotic PtK_2 Cells

Prometaphase cells were fluorescently imaged for various checkpoint components before and after photobleaching of a single kinetochore. Representative FRAP graphs are shown. Mps1, Bub3, Mad1, and Bub1 displayed monophasic recoveries, whereas BubR1 and Cdc20 displayed biphasic recoveries at early prometaphase kinetochores. Mad1 and Bub1, however, were more stable components of unattached kinetochores relative to the other spindle checkpoint proteins. Half-lives and percent recoveries were determined by using Excel and SigmaPlot.

over rates compared to unattached kinetochores (Table 1). For example, Bub3 half-life decreased ~3-fold, Mps1 decreased ~2.6-fold, and Bub1 decreased ~2.3-fold. Although the dynamic fraction of Bub1 turned over faster at metaphase, the large, stable fraction remained the same as for unattached kinetochores, indicating that this fraction of Bub1 remains a stable component of the kinetochore scaffold. Most significantly, the slow kinetic components of Cdc20 disappeared (see below; Table 1).

The Loss of the Slow Component of Cdc20 Dynamics at Metaphase Kinetochores Is Not Tension Dependent

We reasoned that the increased dynamics at metaphase kinetochores might result from the loss of phosphorylation activity that occurs at kinetochores as they come under tension [32–35] or from the loss of protein-protein interactions, e.g., loss of Mad1 and Mad2 at metaphase kinetochores. To test the possibility that increased dynamic exchange is due to loss of tension, we repeated our FRAP analysis of Cdc20 in metaphase cells treated with 10 μM taxol for 45–60 min. Waters et al. [30] and McEwen et al. [36] have shown that near-normal microtubule occupancy is maintained while kinetochore tension is lost in PtK_1 cells after a 45 min incubation in 10 μM taxol. We found Cdc20 displayed a similar turnover at metaphase kinetochores in taxol-treated cells ($t_{1/2}$ of ~2s and ~88% recovery; Figure 4B; Table 1) compared to untreated cells ($t_{1/2}$ of ~2s and ~95% recovery; $p < 0.01$; Figure 4B; Table 1). This result indicates that the

Table 2. Quantitative Measurements of the Percentage of Total Cell Fluorescence at a Single Kinetochore for Various GFP Proteins

	Late Prophase (Pro)	Unattached Prometaphase (UA Prom)	Attached Prometaphase (A Prom)	Late Metaphase (lMeta)	Anaphase (Ana)	Telophase (Telo)
Mps1	0.02 ± 0.005	0.05 ± 0.009	0.02 ± 0.005	0.009 ± 0.003	0.005 ± 0.003	NA
n	6	6	9	8	4	
Bub1	0.05 ± 0.01	0.4 ± 0.18	0.2 ± 0.06	0.04 ± 0.01	0.03 ± 0.01	ND
n	7	5	4	4	4	
Bub3	0.07 ± 0.03	0.15 ± 0.04	0.13 ± 0.05	0.05 ± 0.02	0.03 ± 0.01	0.009 ± 0.002
n	7	7	6	8	5	3
BubR1	NA	0.1 ± 0.05	0.02 ± 0.01	0.004 ± 0.002	NA	NA
n		9	7	4		
Mad1	0.05 ± 0.03	0.03 ± 0.009	0.009 ± 0.002	0.003 ± 0.0009	NA	NA
n	4	9	13	4		
Mad2	0.06 ± 0.01	0.02 ± 0.009	0.001 ± 0.001	NA	NA	NA
n	7	4	15			
Cdc20	0.04 ± 0.01	0.05 ± 0.02	0.04 ± 0.005	0.03 ± 0.005	0.03 ± 0.009	0.01 ± 0.005
n	8	8	11	5	10	5

Integrated fluorescence intensity of individual kinetochores was quantitatively determined on cells expressing low levels of various GFP proteins. For each individual cell, the average kinetochore fluorescence was determined, then divided by the total cell fluorescence after background subtraction, and finally multiplied by 100%. Final percentage values represent the overall mean from all cells measured per experimental condition. Standard deviations are provided. n = number of cells; NA = not applicable; ND = not determined.

absence of the slow kinetic component of Cdc20 turnover at metaphase kinetochores depends on microtubule attachment and not tension.

The Dependence of the Slow Kinetic Fraction of Cdc20 at Unattached Kinetochores on Mad2-Cdc20 Interaction

We were intrigued to find that the slow kinetic component of Cdc20 disappeared at metaphase kinetochores and that only the fast component remained ($t_{1/2}$ of ~2s and ~95% recovery; Table 1). Cdc20 has been shown to bind BubR1 and Mad2 in vitro [8–10]. Since some BubR1 is present on metaphase kinetochores until late metaphase and Mad2 is not, we reasoned the slow component of Cdc20 turnover might be due to interactions with Mad2. To explore this possibility, we examined the turnover rate of a GFP-Cdc20 construct, GFP-$Cdc20_{\Delta 1-167}$, at kinetochores. When examined in cells, Kallio and coworkers showed that GFP-CDC20 coimmunoprecitates with Mad2, while the GFP-$Cdc20_{\Delta 1-167}$ does not [15]. We verified in HeLa cells that GFP-$Cdc20_{\Delta 1-167}$ does not coimmunoprecipitate with Mad2 in vivo (data not shown). When GFP-$Cdc20_{\Delta 1-167}$ and Mad2 were coexpressed in reticulolysates, we found a weak binding by coimmunoprecipitation that was not seen in vivo (Figure 4A). This residual binding in vitro may indicate another Cdc20 binding domain for Mad2, but it could also be the result of misfolding in the in vitro expression system or simply background binding. When expressed in PtK1 cells, we found the slow kinetic component typical of full-length GFP-Cdc20 was not evident when we analyzed the turnover rate of GFP-$Cdc20_{\Delta 1-167}$ at both unattached and attached kinetochores (Figure 4B) in PtK_2 cells. For example, GFP-$Cdc20_{\Delta 1-167}$ displayed a $t_{1/2}$ of 1.5 s with ~94% recovery at prophase kinetochores (data not shown), $t_{1/2}$ of 2.4s with ~93% recovery at prometaphase kinetochores (Table 1), $t_{1/2}$ of 1.7 s with ~91% recovery at metaphase kinetochores (Table 1), and a $t_{1/2}$ of 1.3 s with ~85% recovery at anaphase kinetochores (data not shown). These data suggest that the slow component of Cdc20 kinetics at unattached kinetochores likely represents a subpopulation of Cdc20 that is interacting with Mad2.

Changes in the Levels of Spindle Checkpoint Proteins and Cdc20 at Kinetochores during Mitosis

We quantified the changes in protein levels of the GFP fusion proteins at kinetochores as chromosomes gained microtubule attachments and alignment at the metaphase plate. The GFP fusion with the highest percentage of total cellular fluorescence at kinetochores was GFP-Bub1, which exhibited nearly 0.4% of the total GFP-Bub1 at an unattached prometaphase kinetochore or about 10% at all 26 kinetochores shortly after nuclear envelope breakdown (Table 2). For the other checkpoint proteins and GFP-Cdc20, the maximum percentage of the total GFP-protein pool at an unattached kinetochore was around 0.05%–0.1% (Table 2). The percentages given in the Table 2 likely underestimate the endogenous protein ratios by about a factor of 1.5–5 (see Supplemental Discussion). Nevertheless, the maximum values of the percentages are small and indicate that the vast majority of the checkpoint proteins and Cdc20 are in the cytoplasmic pool and not localized to kinetochores at one point in time. We estimate the number of molecules at unattached kinetochores is on the order of 500–5000 (see Supplemental Discussion).

Unlike our live-cell measurements, previous immunofluorescence assays have been unable to resolve early and late metaphase stages from fixed time-point assays of unsynchronized mitotic populations, e.g., [2]. We found interesting differences that are most easily seen by comparing levels of fluorescence intensities at kinetochores relative to maximum values in early mitosis (Figure 5; Table 2). Mad2 decreased much more quickly from kinetochores compared to Mad1, being >20-fold depleted by early metaphase compared to a 6-fold depletion for Mad1 (Figure 5A′; Table 2). By mid to late

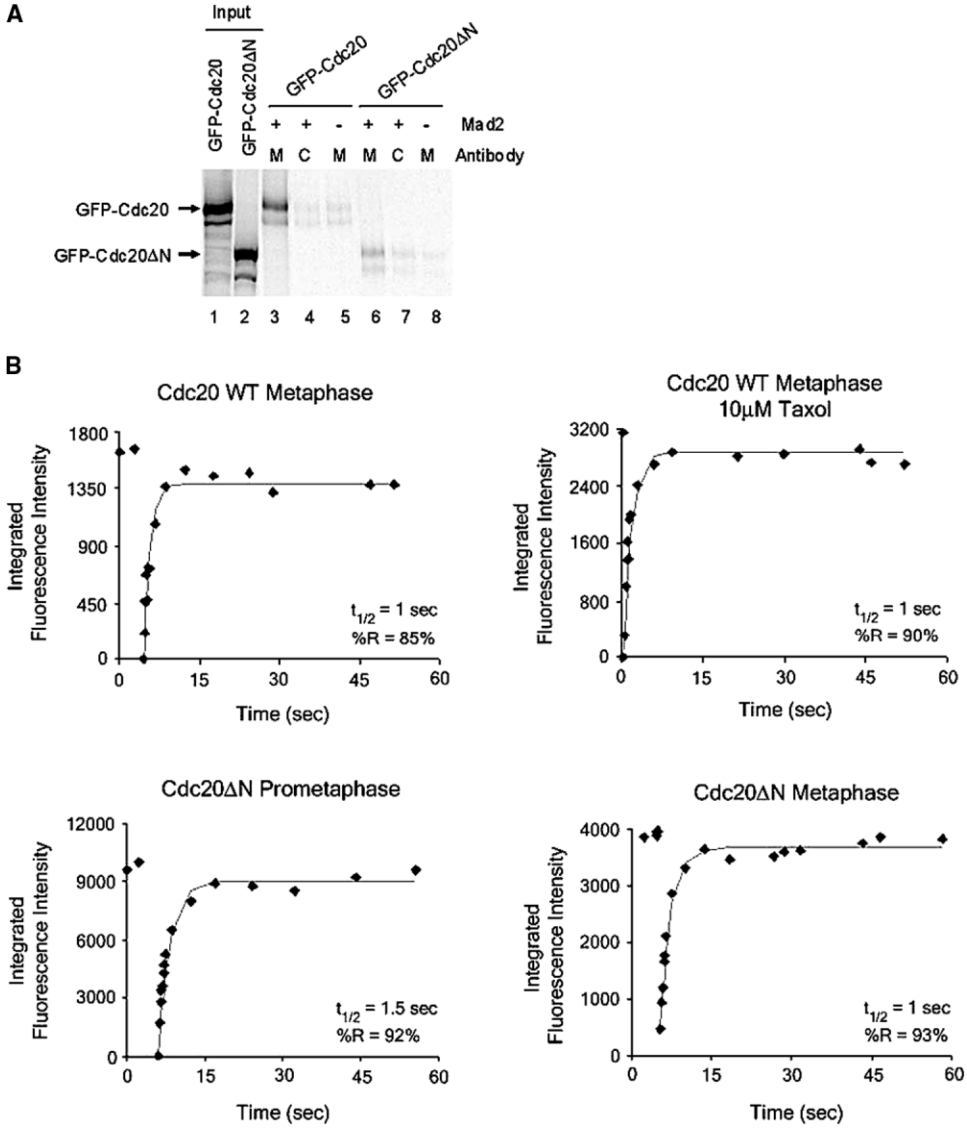

Figure 4. Analysis of GFP-Cdc20 Wild-Type and GFP-Cdc20$_{\Delta 1-167}$ Mutant at Unattached and Attached Kinetochores in Mitotic PtK$_2$ Cells

(A) In vitro binding of GFP-Cdc20 and GFP-Cdc20ΔN to recombinant Mad2. GFP-Cdc20 (lane 1) and GFP-Cdc20ΔN (lane 2) were synthesized in reticulocyte lysates in the presence of [35S]-Met in vitro. Labeled proteins were incubated with recombinant Mad2 (lanes 3, 4, 6, and 7) or with a buffer (lanes 5 and 8). The Mad2 complexes were then immunoprecipitated by an affinity-purified anti-Mad2 antibody (M, lanes 3, 5, 6, and 8) or with a control IgG (C, lanes 4 and 7), and associated GFP-Cdc20 and GFP-Cdc20ΔN were analyzed by SDS-PAGE. GFP-Cdc20 has a much higher affinity to Mad2 than GFP-Cdc20ΔN.

(B) Wild-type GFP-Cdc20 displayed a similar turnover rate at metaphase kinetochores in untreated cells compared to metaphase kinetochores in taxol-treated cells ($t_{1/2} = \sim$1s). GFP-Cdc20ΔN displayed a single, fast recovery at both unattached prometaphase and attached metaphase kinetochores.

metaphase, Mad1 became greater than 20-fold depleted like Mad2 (Table 2). BubR1 was reduced only 4.2-fold in early metaphase and then became reduced by >20-fold in late metaphase (Figure 5A; Table 2). The normalized reduction of Bub3 by anaphase was much less than seen for either BubR1 or Bub1 (Figure 5A; Table 2). Also, Mps1 decreased by about 5-fold by late metaphase and persisted at this level into anaphase (Figure 5A′; Table 2). Finally, Cdc20 decreased by 1.5-fold in early metaphase, 1.7-fold in late metaphase, and remained constant between late metaphase and most of anaphase (Figure 5A′; Table 2), similar to the recent findings by Kallio et al. [15] for LLPCK cells. Also, the fraction of Cdc20 that disappears from kinetochores between prometaphase and late metaphase (fluorescence prometaphase minus fluorescence late metaphase) has a similar time-course to that exhibited by the loss of MCC components Mad2, BubR1, and Bub3 (Figure 5B). These comparisons and the biphasic character of Cdc20 FRAP suggest that at unattached kinetochores there are two fractions of Cdc20: a slow fraction that depletes with checkpoint inactivation and a fast fraction that does not.

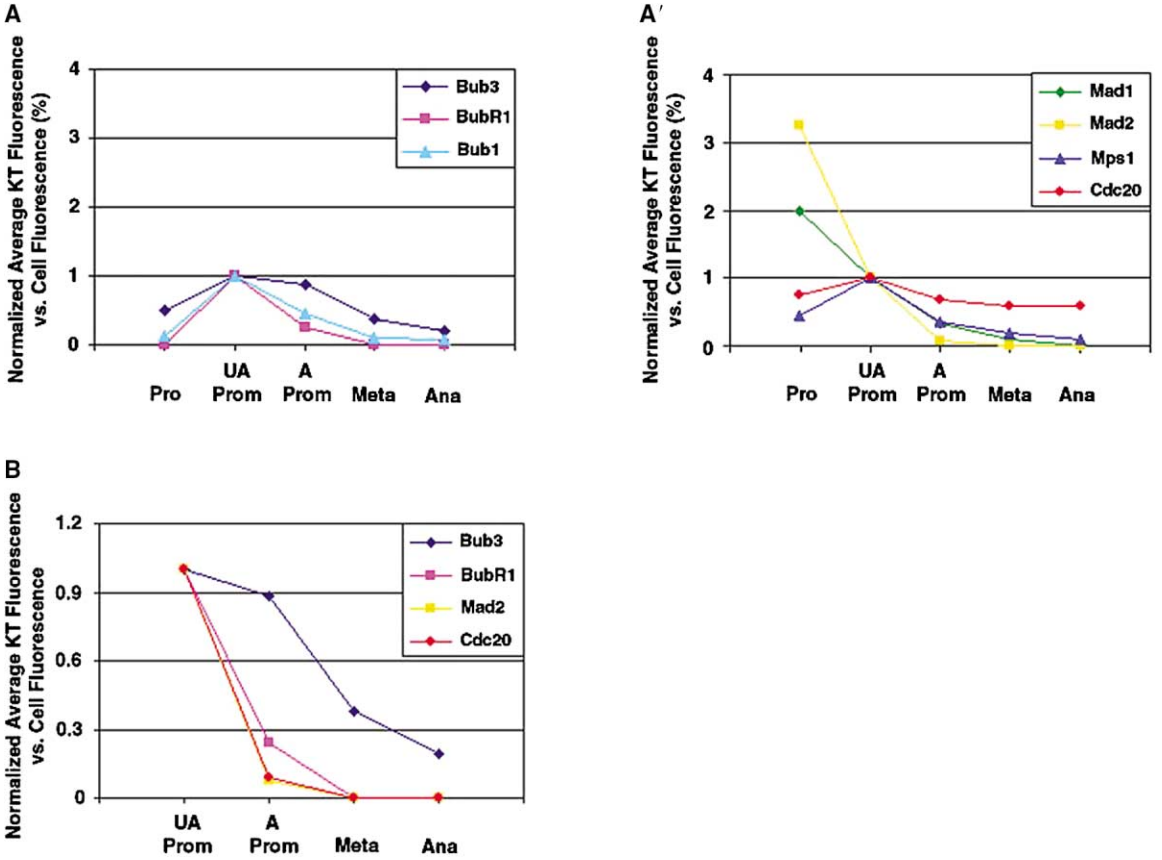

Figure 5. Quantification of Kinetochore Fluorescence for GFP Fusions to the Spindle Checkpoint Proteins and Cdc20

(A and A′) Kinetochore fluorescent intensity measurements for each of the spindle checkpoint proteins and Cdc20 in Table 2 were normalized to their respective fluorescent intensities at unattached, early prometaphase kinetochores, and plotted.

(B) Comparison of changes in kinetochore fluorescence intensity for Cdc20 (red) relative to the steady value of Cdc20 at late metaphase through anaphase against changes in fluorescence intensities observed for the MCC components Mad2 (yellow), BubR1 (pink), and Bub3 (blue) from prometaphase to late metaphase taken from Figures 2B and 2B′. Actual values are reported in Table 2.

Discussion

Mad1 and Bub1 Are Relatively Stable Components of the Kinetochore While Most Mad2, BubR1, Bub3, and Mps1 Cycle Much More Rapidly through the Kinetochore

In this study, we use FRAP techniques to show that Mad2, BubR1, Bub3, Cdc20, and Mps1 cycle rapidly through unattached kinetochores, whereas most Bub1 and Mad1 are much more stable. Mad1 is known to recruit Mad2, and although a large fraction of Mad1 is bound tightly to Mad2 in the cytoplasm [37, 38], our FRAP measurements indicate that 70% of Mad1 is stable at unattached kinetochores while about 90% of Mad2 is cycling through with a half-life of about 20 s (Table 1). In addition, during chromosome alignment, Mad2 decreases more rapidly at kinetochores than Mad1 (Figure 5A′; Table 2). These results demonstrate that the Mad1 needed to target Mad2 to kinetochores is mainly resident at the kinetochore, while the cytoplasmic Mad2 that exchanges rapidly at kinetochores is mainly free of Mad1. This result is supported by studies in *Xenopus* egg extracts that show Mad1-free Mad2 is essential for kinetochore-dependent spindle checkpoint activity [38]. When Mad1 is bound to kinetochores, as in prometaphase, Mad1 localizes strongly to the proximal spindle fibers and spindle poles (Figure 1) most likely because of the dynein/dynactin-dependent transport from kinetochore to poles as identified previously for Mad2 and its binding site [18, 39]. This transport may also drive the small fraction of Mad1 turnover we observed at unattached kinetochores (Figures 3 and S5).

It has previously been documented that Mps1 is needed for Mad1/Mad2 binding to kinetochores [23, 24]. Interestingly, our results indicate Mad1 is much more stable at kinetochores than Mps1, suggesting Mps1 can leave kinetochores without Mad1. Therefore, other proteins must be present at kinetochores (other than Mps1) and provide a binding site(s) for Mad1. Mps1 has been shown to phosphorylate Mad1; therefore, phosphorylation of Mad1 may stabilize Mad1 binding to another site on the kinetochore. Bub1, like Mad1, is not likely a component of the diffusible wait-anaphase signal because a large fraction is stable at unattached kinetochores and the dynamic fractions have a long average half-life, 57 s. A major role for Bub1, like Mad1, may be to provide a protein scaffold at kinetochores to support the binding [26, 37, 40, 41] and cycling of Bub1 free Bub3 and BubR1.

Although BubR1-Bub1 and Bub3-Bub1 are constitu-

tive complexes in the cytoplasm [4], our results indicate that these complexes are not dynamically exchanging at kinetochores. This is because 100% of BubR1 and 95% of Bub3 cycle through unattached kinetochores much faster than even the dynamic fraction of Bub1.

BubR1 is a major candidate molecule for the diffusible wait-anaphase signal since it is a direct inhibitor of APC/C^{Cdc20} in in vitro assays [9, 10]. We find that BubR1 exhibits two dynamic populations at unattached kinetochores: about 54% cycles through unattached kinetochores with a half-life of 21 s, which is similar to Bub3, a known binding partner. About 46% have a much faster half-life, 3 s, and must be cycling through the kinetochore independent of Bub3. Either the faster or slower kinetic component of BubR1 could be part of the diffusible wait-anaphase signal. Our live-cell analysis shows that BubR1 is reduced at kinetochores as they become aligned in two stages. The initial 4-fold loss of BubR1 at early metaphase kinetochores (Figure 5A; Table 2) is most likely produced by kinetochore microtubule formation, since treating metaphase cells with taxol to produce loss of tension without detachment, produces a slight, although significant, elevation of kinetochore BubR1 levels [2, 35]. The further 5-fold loss of kinetochore BubR1 by anaphase (Figure 5A; Table 2) may be caused by a slow kinetochore response to persistent kinetochore tension [35, 42]. It should be noted that BubR1 behavior at kinetochores differs from Mad2 in that by overexpressing GFP-BubR1, we were able to see cells enter anaphase with greatly reduced but detectable levels of BubR1 at kinetochores (Figure S6). In contrast, cells overexpressing Mad2 did not enter anaphase with detectable Mad2 at metaphase kinetochores (data not shown) [18]. Therefore, BubR1 is not as substantially depleted from kinetochores as Mad2 for spindle checkpoint inactivation at anaphase onset.

Bub3 persists at much higher concentrations at metaphase and anaphase kinetochores than either Bub1 or BubR1 (Figure 5A; Table 2). This indicates that both Bub1 and BubR1 can leave kinetochores without a corresponding loss in kinetochore Bub3 and that a binding site exists for Bub3 at kinetochores that does not require Bub3 to be bound to either BubR1 or Bub1. This other binding site may be associated somehow with Mad1/Mad2 since Bub3, but not Bub1 or BubR1, is seen at spindle poles when Mad1/Mad2 is present on kinetochores (Figure 1).

The Kinetics of about Half of Cdc20 at Unattached Kinetochores Appear to Depend on Mad2 Interactions

About 50% of Cdc20 at unattached prometaphase kinetochores exhibit a half-life of 23 s (nearly identical to the 19 s half-life of Mad2) and 50% exhibit a half-life of 1–2 s (Table 1). The slow phase of Cdc20 kinetics is likely not due to interactions with BubR1, because prophase kinetochores exhibit almost identical Cdc20 kinetics yet have no measurable BubR1 (Figures 1 and 5; Table 2). The slow phase appears to depend on interactions with kinetochore bound Mad2 for several reasons. The slow phase disappears by metaphase when kinetochores are depleted of Mad2. Its disappearance does not depend on the tension generated at metaphase kinetochores, because it does not reappear when metaphase spindles are treated with taxol to produce loss of tension without loss of kinetochore microtubules or reappearance of kinetochore Mad2 (Figure 5A′;Table 2) [30, 36]. The slow phase in Cdc20 kinetics was also absent for GFP-$Cdc20_{\Delta 1-167}$ bound to unattached kinetochores in prophase, prometaphase, and nocodazole-treated cells, a mutant with diminished Mad2 interactions. These kinetochores have high concentrations of Mad2 and kinetics similar to the slow phase of full-length Cdc20. Lastly, we found Cdc20 localizes strongly to spindle poles in PtK_2 cells when Mad1/Mad2 is concentrated at proximal kinetochores, and Cdc20 displays little to no pole localization during metaphase despite elevated levels of Cdc20 on metaphase kinetochores. This suggests that the Cdc20 that is transported poleward is associated with Mad1/Mad2. Taken together, these results strongly suggest Cdc20 interacts with Mad2 at the kinetochore.

Models for Generation of the Diffusible Wait-Anaphase Signal

The Catalytic Model for Formation of MCC or Its Subcomplexes

One interpretation of our data is that the kinetochore catalyzes the formation of the Mad2-Cdc20 complex from Cdc20 and Mad2 [15] with the following features (Figure 6, model 1). The correspondence of the slow phase kinetics of Cdc20 with the single phase of Mad2 and the effects of the nonbinding Cdc20 mutant suggests, although does not prove, that half of the Cdc20 at the kinetochore is bound to Mad2. The other 50% of Cdc20 that binds to the kinetochore does not bind Mad2 and rapidly dissociates with a half-life of 1–2 s. Cdc20-BubR1-Bub3 or the entire MCC complex could be forming at kinetochores (Figure 6, model 1) since about 50% of BubR1 and the great majority of Bub3 exhibit kinetochore half-lives of about 19–23 s, similar to that of Mad2 and the slow component of Cdc20. However, our data indicate that the kinetics of Cdc20 does not depend on either BubR1 or Bub3 as it does for Mad2.

Positive-Feedback Models of Kinetochore-Modified Cdc20, BubR1, or Mps1 as Diffusible Inhibitors of APC/C Activation in the Cytoplasm

Kinetochore modification of Cdc20, BubR1, or Mps1 is attractive to consider for the diffusible wait-anaphase signal because they all have components that exhibit rapid cycling through the kinetochore: half-lives of 1–3 s for Cdc20 and BubR1 and 13 s for Mps1. Kinetochore modified Cdc20*, BubR1*, or Mps1* could diffuse into the cytoplasm and promote formation of Cdc20-Mad2, Cdc20-BubR1-Bub3, or the entire MCC from pools of Mad1-Mad2, BubR1-Bub1, or Bub3-Bub1 (Figure 6, model 2). Mps1* may also inhibit APC/C perhaps through phosphorylation as proposed by Liu et al. [23]. MCC or its subcomplexes could then provide a positive feedback mechanism by binding kinetochores that lack microtubules [30, 35, 43] and stimulating further production of Cdc20*, BubR1*, or Mps1*. This feedback mechanism would account for a Mad2-dependent slow phase in Cdc20 kinetics at checkpoint active kinetochores that is lost with kinetochore alignment. Another attractive feature of this model for our data is that it accounts for why kinetochores with high checkpoint

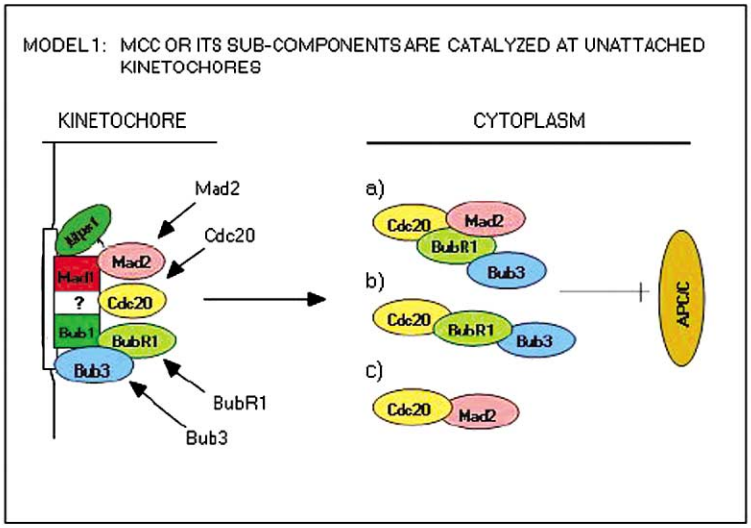

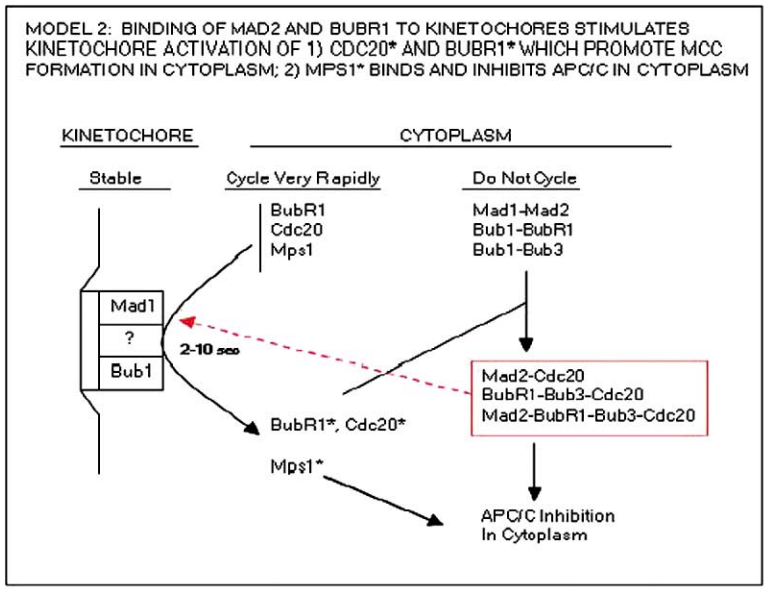

Figure 6. Possible Models Predicted by Our FRAP Data and Kinetochore Fluorescence Quantification

Model one shows the kinetochore catalytic model. Mad2, BubR1, and Bub3 are combined at the kinetochore with Cdc20 and released into the cytoplasm as MCC or its subcomplexes, Mad2-Cdc20, BubR1-Bub3-Cdc20, or Mad2-Cdc20-Bub3-BubR1, where they inhibit APC/C activation.

Model two shows Kinetochore activation of Cdc20, BubR1, or Mps1 for the diffusible wait-anaphase signal. In this positive-feedback model, kinetochore binding of Mad2 or BubR1 complexes activates kinetochore formation of Cdc20*, BubR1*, or Mps1*, which diffuse into the cytoplasm and induce the formation of MCC or the Mad2-Cdc20 and the BubR1-Bub3-Cdc20 subcomplexes (red box) from cytoplasmic pools of Mad1-Mad2, Bub1-BubR1, and Bub1-Bub3. Unattached kinetochores may also activate and promote the ability of Mps1* to phosphorylate APC/C in the cytoplasm and sensitize the APC/C to inhibition by MCC components.

activity in nocodazole all have high concentrations of Cdc20, BubR1, and Mad2 in a cytoplasm where MCC and its subcomplexes are in their highest concentration. It also provides an explanation for how a single unattached kinetochore could maintain high checkpoint activity without the products of checkpoint activation, MCC, and its subcomplexes, inhibiting product production.

Conclusions

Most Mad1 and Bub1 are relatively stable components of the kinetochore and are not likely part of the diffusible wait-anaphase signal. Both inhibitors of Cdc20, BubR1, and Mad2, cycle rapidly through unattached kinetochores and are substantially depleted on kinetochores of properly aligned chromosomes. Cdc20 also cycles rapidly through kinetochores, and we provide evidence that 50% of the Cdc20 bound to unattached kinetochores are bound to Mad2, and that this fraction dissociates from the kinetochores with the kinetics exhibited by other components of the MCC, BubR1, and Bub3. This data supports a catalytic model where the kinetochore promotes the production of Cdc20-Mad2 or Cdc20-MCC components at the kinetochore. The fast kinetics of Cdc20, BubR1, and Mps1 also support a model in which kinetochores modify these components to promote the formation of Cdc20 inhibitory complexes in the cytoplasm.

Experimental Procedures

GFP Constructs and Expression

The full-length coding sequence for human proteins of Mps1, Bub1, Bub3, BubR1, Mad2, Cdc20, APC10, and APC11 were blunt ended and subcloned into the pCS2-GFP mammalian expression vector (a gift from Dr. Robert Davis at Harvard Medical School) so that the GFP fusion gene was at the amino terminal end of the proteins.

The C terminus of Mad1 was fused to the GFP in pCS2, since the N-terminal fusion interferes the folding of the Mad1. PtK_2 cells (ATCC) were cultured and transfected by using FuGENE6 (Roche) following manufacturers instructions and imaged 48–72 hr post-transfection [18]. HeLa cells were cultured and transfected as described in Fang et al. [44]. For microinjection studies, polyclonal GFP antibodies (Molecular Probes) were dialyzed into injection buffer (20 mM HEPES, 100 mM KCl, 0.5 mM $MgCl_2$ [pH 7.5–7.7]) and injected into cells at 0.5 mg/ml (needle concentration).

Western Blots and Immunoprecipitation Assays

HeLa cells were transfected via Effectene (Qiagen) with plasmids expressing either GFP, GFP-APC/C10, or GFP-APC/C11 (GFP-pCS2, GFP-APC/C10-pCS2, or GFP-APC/C11-pCS2, respectively). 60 hr posttransfection cells were harvested and extracts were prepared and immunoprecipitated with affinity-purified poly-clonal Cdc27 antibodies or nonimmune IgG covalently coupled to AffiPrep-Protein A beads (BioRad) essentially as described in [44]. Immune-complexes and whole-cell extracts were separated by SDS-PAGE, transferred to nitrocellulose, and probed with GFP and Cdc27 antibodies.

Microscopy and Laser Photobleaching

For fluorescence and phase microscopy studies, cells were placed in modified Rose chambers and imaged on a Nikon TE300 inverted microscope as described previously [18, 39]. Photobleaching experiments were performed essentially as described previously [18, 39]. For Cdc20 and BubR1 photobleaching experiments, images were collected during a 2 s streaming period in which the camera was run at five to eight frames per second, and photobleaching of single kinetochores was performed during this acquisition time. Subsequent images were collected at various time intervals depending on the experiment, ranging from one frame per 2–60 s, with exposure times of 150–300ms. MetaMorph software was used to measure integrated fluorescence intensities of kinetochores, as described previously [18]. The exponential kinetics of FRAP were analyzed by calculating the normalized unrecovered fluorescence at each time point, $(F_{inf} - F_{(t)})/(F_{inf} - F_0)$, where F_{inf} is the average maximal fluorescence recovery, and F_0 is the fluorescence immediately after photobleaching [18, 39]. The normalized data was fit to either $\exp(-kt)$ from the slope of the ln plot of the normalized data Microsoft Excel or fit to a double exponential, $R_f\exp(-k_f t) + R_s\exp(-k_s t)$ by using the Regression Wizard function in SigmaPlot, where f and s are the fast and slow components, respectively.

Quantitation of GFP Fusion Protein Levels at Kinetochores

Only PtK_2 cells expressing GFP chimeras barely detectable by eye in the microscope were recorded and used for the experiments described in this paper. We found cells expressing low levels of GFP-fusion proteins exhibited normal progression through mitosis, and anaphase onset occurred $\sim$68 $\pm$ 31 min (n = 17 cells) after nuclear envelope breakdown. These cells entered anaphase $\sim$12 $\pm$ 5 min after the last chromosome congressed to the metaphase plate, consistent with previous studies in PtK_1 cells [18]. Overall, we found $<$5% of the cells observed spent $>$2 hr in mitosis, but in cases which this occurred, it was due to a delay in biorientation and congression of the last monooriented chromosome to the metaphase plate. Cell expressing GFP fusions had an average total integrated cellular GFP fluorescence (see below) of about 25 $\pm$ 15 $\times$ 10^6 photon counts. Chromosome position was used to identify mitotic stage and therefore our measurements assume that all kinetochores were in a similar state when measured; e.g., (1) unattached, untense versus (2) partially attached, partially tense versus (3) fully attached, fully tense.

To obtain estimates of the ratio between steady-state kinetochore protein levels compared to total cytoplasmic pools, we measured the integrated GFP fluorescence for the spindle checkpoint and Cdc20 proteins at kinetochores relative to the total cellular fluorescence at the different stages of mitosis. Briefly, integrated GFP chimera fluorescence intensities at kinetochores were measured within a 10 $\times$ 10 pixel circle followed by background subtraction from a larger 16 $\times$ 16 pixel circle of the same region [18, 39]. Total cell fluorescence was obtained by measuring integrated fluorescence throughout the cell boundary in the same plane kinetochores were analyzed, followed by background subtraction by using integrated fluorescence intensity measurements from a 25 $\times$ 25 pixel circle outside the cell that was then used to calculate the ratio between the two areas. For each cell, the average kinetochore fluorescence intensity was measured, multiplied by 22 (number of kinetochores in a PtK_2 cell), divided by the overall cell fluorescence, and multiplied by 100%. These average values were then used to calculate an overall mean value for percent of total kinetochore fluorescence versus cell fluorescence (with 3–15 cells measured per mitotic stage and 3–22 kinetochores measured per cell; Table 2). Therefore, the actual percentage of fluorescence signal contributed from a single kinetochore can be derived by dividing this percentage value by 22. Since PtK_2 cells remain relatively flat on poly-L-lysine coverslips throughout mitosis, we believe our estimates are fair comparisons between the various mitotic stages.

Supplemental Data

Supplemental Data including a Supplemental Discussion section, six figures, and five movies are available at http://www.current-biology.com/cgi/content/full/14/11/953/DC1/.

Acknowledgments

We thank James Chen for constructing GFP fusion genes. This work was supported by ACS Postdoctoral Fellowship (00-147-01-CCG) to B.J.H., a Tumor Biology Training Grant from the National Institutes of Health (NIH) to S.S. (CA09151), and NIH grants to E.D.S. (GM-24364) and G.F. (GM62852). G.F. is a Searle Scholar, a Kimmel Scholar in Cancer Research, a recipient of the Beckman Young Investigator Award, and a recipient of the Burroughs-Wellcome Career Award in Biomedical Sciences.

Received: November 26, 2003
Revised: May 18, 2004
Accepted: May 19, 2004
Published: June 8, 2004

References

1. Jallepalli, P.V., and Lengauer, C. (2001). Chromosome segregation and cancer: cutting through the mystery. Nat. Rev. Cancer *1*, 109–117.
2. Hoffman, D.B., Pearson, C.G., Yen, T.J., Howell, B.J., and Salmon, E.D. (2001). Microtubule dependent changes in the assembly of microtubule motor proteins and mitotic spindle checkpoint proteins in PtK_1 kinetochores. Mol. Biol. Cell *12*, 1995–2009.
3. Millband, D.N., Campbell, L., and Hardwick, K.G. (2002). The awesome power of multiple model systems: interpreting the complex nature of spindle checkpoint signaling. Trends Cell Biol. *12*, 205–209.
4. Musacchio, A., and Hardwick, K.G. (2002). The spindle checkpoint: structural insights into dynamic signaling. Nat. Rev. Mol. Cell Biol. *3*, 731–741.
5. Rieder, C.L., and Salmon, E.D. (1998). The vertebrate cell kinetochore and its roles during mitosis. Trends Cell Biol. *8*, 310–318.
6. Hwang, L.H., Lau, L.F., Smith, D.L., Mistrot, C.A., Hardwick, K.G., Hwang, E.S., Amon, A., and Murray, A.W. (1998). Budding yeast Cdc20: a target of the spindle checkpoint. Science *279*, 1041–1044.
7. Kim, S.H., Lin, D.P., Matsumoto, S., Kitazono, A., and Matsumoto, T. (1998). Fission yeast Slp1: an effector of the Mad2-dependent spindle checkpoint. Science *279*, 1045–1047.
8. Fang, G., Yu, H., and Kirschner, M.W. (1998). The checkpoint protein MAD2 and the mitotic regulator CDC20 form a ternary complex with the anaphase-promoting complex to control anaphase initiation. Genes Dev. *12*, 1871–1883.
9. Tang, Z., Bharadwaj, R., Li, B., and Yu, H. (2001). Mad2-independent inhibition of APC^{Cdc20} by the mitotic checkpoint protein BubR1. Dev. Cell *1*, 227–237.
10. Fang, G. (2002). The checkpoint protein BubR1 acts synergisti-

cally with Mad2 to inhibit anaphase-promoting complex. Mol. Biol. Cell *13*, 755–766.
11. Sudakin, V., Chan, G.K.T., and Yen, T.J. (2001). Checkpoint inhibition of the APC/C in HeLa cells is mediated by a complex of BUBR1, BUB3, CDC20 and MAD2. J. Cell Biol. *154*, 925–936.
12. Millband, D.N., and Hardwick, K.G. (2002). Fission yeast Mad3p is required for Mad2p to inhibit the anaphase-promoting complex and localizes to kinetochores in a Bub1p-, Bub3p-, and Mph1p-dependent manner. Mol. Cell. Biol. *22*, 2728–2742.
13. Chen, R.-H. (2002). BubR1 is essential for kinetochore localization of other spindle checkpoint proteins and its phosphorylation requires Mad1. J. Cell Biol. *158*, 487–496.
14. Kallio, M., Weinstein, J., Daum, J.R., Burke, D.J., and Gorbsky, G.J. (1998). Mammalian p55CDC mediates association of the spindle checkpoint protein Mad2 with the cyclosome/anaphase-promoting complex, and is involved in regulating anaphase onset and late mitotic events. J. Cell Biol. *141*, 1393–1406.
15. Kallio, M.J., Beardmore, V.A., Weinstein, J., and Gorbsky, G.J. (2002). Rapid microtubule-independent dynamics of Cdc20 at kinetochores and centrosomes in mammalian cells. J. Cell Biol. *158*, 841–847.
16. Yu, H. (2002). Regulation of APC-Cdc20 by the spindle checkpoint. Curr. Opin. Cell Biol. *14*, 706–714.
17. Gorbsky, G.J., Chen, R.-H., and Murray, A.W. (1998). Microinjection of antibody to Mad2 protein into mammalian cells in mitosis induces premature anaphase. J. Cell Biol. *141*, 1193–1205.
18. Howell, B.J., Hoffman, D.B., Fang, G., Murray, A.W., and Salmon, E.D. (2000). Visualization of Mad2 dynamics at kinetochores, along spindle fibers, and at spindle poles in living cells. J. Cell Biol. *150*, 1233–1249.
19. Tugendreich, S., Tomkiel, J., Earnshaw, W., and Heiter, P. (1995). Cdc27hs colocalizes with cdc16hs to the centrosome and mitotic spindle and is essential for the metaphase to anaphase transition. Cell *81*, 261–268.
20. Jorgensen, P.M., Brundell, E., Starborg, M., and Hoog, C. (1998). A subunit of the anaphase-promoting complex is a centromere-associated protein in mammalian cells. Mol. Cell. Biol. *18*, 468–476.
21. Topper, L.M., Campbell, M.S., Tugendreich, S., Daum, J.R., Burke, D.J., Hieter, P., and Gorbsky, G.J. (2002). The dephosphorylated form of the anaphase-promoting complex protein Cdc27/Apc3 concentrates on kinetochores and chromosome arms in mitosis. Cell Cycle *1*, 282–292.
22. Huang, J., and Raff, J.W. (2002). The dynamic localisation of the *Drosophila* APC/C: evidence for the existence of multiple complexes that perform distinct functions and are differentially localised. J. Cell Sci. *115*, 2847–2856.
23. Liu, S.-T., Chan, G.K.T., Hittle, J.C., Fujii, G., Lees, E., and Yen, T.J. (2003). Human Mps1 kinase is required for mitotic arrest induced by the loss of CENP-E from kinetochores. Mol. Biol. Cell *14*, 1638–1651.
24. Abrieu, A., Magnaghi-Jaulin, L., Kahana, J.A., Peter, M., Castro, A., Vigneron, S., Lorca, T., Cleveland, D.W., and Labbe, J.C. (2001). Mps1 is a kinetochore-associated kinase essential for the vertebrate mitotic checkpoint. Cell *106*, 83–93.
25. Bulinski, J.C., Odde, D.J., Howell, B.J., Salmon, T.D., and Waterman-Storer, C.M. (2001). Rapid dynamics of the microtubule binding of ensconsin in vivo. J. Cell Sci. *114*, 3885–3897.
26. Taylor, S.S., Ha, E., and McKeon, F. (1998). The human homologue of Bub3 is required for kinetochore localization of Bub1 and a Mad3/Bub1-related protein kinase. J. Cell Biol. *142*, 1–11.
27. Jablsonki, S.A., Chan, G.K.T., Cooke, C.A., Earnshaw, W.C., and Yen, T.J. (1998). The hBUB1 and hBUBR1 kinases sequentially assemble onto kinetochores during prophase with hBUBR1 concentrating at the kinetochore plates in mitosis. Chromosoma *11*, 386–396.
28. Stucke, V.M., Sillje, H.H.W., Arnaud, L., and Nigg, E.A. (2002). Human Mps1 kinase is required for the spindle assembly checkpoint but not for centrosome duplication. EMBO J. *21*, 1723–1732.
39. Taylor, S.S., Hussein, D., Wang, Y., Elderkin, S., and Morrow, C.J. (2002). Kinetochore localisation and phosphorylation of the mitotic checkpoint components Bub1 and BubR1 are differentially regulated by spindle events in human cells. J. Cell Sci. *114*, 4385–4395.
30. Waters, J.C., Chen, R.-H., Murray, A.W., and Salmon, E.D. (1998). Localization of Mad2 to kinetochores depends on microtubule attachment, not tension. J. Cell Biol. *141*, 1181–1191.
31. Fisk, H.A., and Winey, M. (2001). The mouse Mps1p-like kinase regulates centrosome duplication. Cell *106*, 95–104.
32. Gorbsky, G.J., and Ricketts, W.A. (1993). Differential expression of a phosphoepitope at the kinetochores of moving chromosomes. J. Cell Biol. *122*, 1311–1321.
33. Nicklas, R.B., Ward, S.C., and Gorbsky, G.J. (1995). Kinetochore chemistry is sensitive to tension and may link mitotic forces to a cell cycle checkpoint. J. Cell Biol. *130*, 929–939.
34. Nicklas, R.B., Campbell, M.S., Ward, S.C., and Gorbsky, G.J. (1998). Tension-sensitive kinetochore phosphorylation in vitro. J. Cell Sci. *111*, 3189–3196.
35. Shannon, K.B., Canman, J.C., and Salmon, E.D. (2002). Mad2 and BubR1 function in a single checkpoint pathway that responds to a loss of tension. Mol. Biol. Cell *13*, 3706–3719.
36. McEwen, B.F., Heagle, A.B., Cassels, G.O., Buttle, K.F., and Rieder, C.L. (1997). Kinetochore fiber maturation in PtK1 cells and its implications for the mechanisms of chromosome congression and anaphase onset. J. Cell Biol. *137*, 1567–1580.
37. Chen, R.-H., Shevchenko, A., Mann, M., and Murray, A.W. (1998). Spindle checkpoint protein Xmad1 recruits Xmad2 to unattached kinetochores. J. Cell Biol. *143*, 283–295.
38. Chung, E., and Chen, R.H. (2002). Spindle checkpoint requires Mad1-bound and Mad1-free Mad2. Mol. Biol. Cell *13*, 1501–1511.
39. Howell, B.J., McEwen, B.F., Canman, J.C., Hoffman, D.B., Farrar, E.M., Rieder, C.L., and Salmon, E.D. (2001). Cytoplasmic dynein/dynactin drives kinetochore protein transport to the spindle poles and has a role in mitotic spindle checkpoint inactivation. J. Cell Biol. *155*, 1159–1172.
40. Basu, J., Logarinho, E., Herrmann, S., Bousbaa, H., Li, Z., Ghan, G.K., Yen, T.J., Sunkel, C.E., and Goldberg, M.L. (1998). Localization of the Drosophila checkpoint control protein Bub3 to the kinetochore requires Bub1 but not Zw10 or Rod. Chromosoma *107*, 376–385.
41. Sharp-Baker, H., and Chen, R.H. (2001). Spindle checkpoint protein Bub1 is required for kinetochore localization of Mad1, Mad2, Bub3, and CENP-E, independently of its kinase activity. J. Cell Biol. *153*, 1239–1250.
42. Nicklas, R.B., Waters, J.C., Salmon, E.D., and Ward, S.C. (2001). Checkpoint signals in grasshopper meiosis are sensitive to microtubule attachment, but tension is still essential. J. Cell Sci. *114*, 4173–4183.
43. Skoufias, D.A., Andreassen, P.R., Lacroix, F.B., Wilson, L., and Margolis, R.L. (2001). Mammalian mad2 and bub1/bubR1 recognize distinct spindle-attachment and kinetochore-tension checkpoints. Proc. Natl. Acad. Sci. USA *98*, 4492–4497.
44. Fang, G., Yu, H., and Kirschner, M.W. (1998b). Direct binding of CDC20 protein family members activates the anaphase-promoting complex in mitosis and G1. Mol. Cell *2*, 163–171.

Note Added in Proof

We call your attention to another paper in this issue that also addresses the dynamics of spindle checkpoint proteins at kinetochores.

Shah, J.V., Botvinick, E., Bonday, Z., Furnari, F., Berns, M., and Cleveland, D.W. (2004). Dynamics of centromere and kinetochore proteins: implications for checkpoint signaling and silencing. Current Biology *14*, 942–952.